Open access • Journal Article • DOI:10.1016/J.SAB.2016.03.005

Innovative combination of spectroscopic techniques to reveal nanoparticle fate in a crop plant — Source link

Camille Larue, Hiram Castillo-Michel, Ricardo J. Stein, Barbara Fayard ...+8 more authors

Institutions: Ruhr University Bochum, European Synchrotron Radiation Facility, University of Grenoble

Published on: 01 May 2016 - Spectrochimica Acta Part B: Atomic Spectroscopy (Elsevier)

Innovative combination of spectroscopic techniques to reveal nanoparticle fate in a crop plant

Camille Larue, Hiram Castillo-Michel, Ricardo Stein, Barbara Fayard, Emeline Pouyet, Julie Villanova, Valérie Magnin, Ana-Elena Pradas del Real, Nicolas Trcera, Samuel Legros, et al.

Innovative combination of spectroscopic techniques to reveal nanoparticle fate in a crop plant

Camille Larue[a*], Hiram Castillo-Michel[b], Ricardo J. Stein[c], Barbara Fayard[d,e], Emeline Pouyet[b], Julie Villanova[f], Valérie Magnin[a], Ana-Elena Pradas del Real[a], Nicolas Trcera[g], Samuel Legros[h], Stéphanie Sorieul[i], Géraldine Sarret[a]

[a]ISTerre, Université Grenoble Alpes, CNRS, F-38041 Grenoble, France. camille.larue@ensat.fr, valerie.magnin@univ-grenoble-alpes.fr, geraldine.sarret@univ-grenoble-alpes.fr, ana.pradas@univ-grenoble-alpes.fr

[b]ESRF, beamline ID21, Grenoble, France. castillo@esrf.fr, emeline.pouyet@esrf.fr

[c]Department of Plant Physiology, Ruhr University Bochum, Universitätsstrasse 150, 44801 Bochum, Germany. ricardo.stein@rub.de

[d]LPS CNRS UMR 8502 - Université Paris Sud Bât 510 - F-91405 Orsay cedex.

[e]Actual adress : Novitom - 1, place Firmin Gautier -F-38000 Grenoble. barbara.fayard@novitom.com

[f]ID16B, ESRF - The European synchrotron, CS40220 38043 Grenoble Cedex 9, France. julie.villanova@esrf.fr

[g]Synchrotron SOLEIL, Gif-sur-Yvette F-91192, France. nicolas.trcera@synchrotron-soleil.fr

[h]CEA/LITEN/DTNM/L2T, CEA Grenoble, Av des Martyrs, 38054 Grenoble Cedex 9, France. samuel.legros@cirad.fr

[i]Université Bordeaux, CNRS/IN2P3, Centre d'Etudes Nucléaires de Bordeaux Gradignan, CENBG, Chemin du Solarium, BP120, 33175 Gradignan, France. sorieul@cenbg.in2p3.fr

* corresponding author : camille.larue@ensat.fr

Present address: CNRS; EcoLab; 31326 Castanet Tolosan, France

Abstract

Nanotechnology is the new industrial revolution of our century. Its development leads to an increasing use of nanoparticles and thus to their dissemination. Their fate in the environment is of great concern and especially their possible transfer in trophic chains might be an issue for food safety. However, so far our knowledge on this topic has been restricted by the lack of appropriate techniques to characterize their behavior in complex matrixes. Here, we present in detail the use of cutting-edge beam-based techniques for nanoparticle *in situ* localization, quantification and speciation in a crop plant species (*Lactuca sativa*). Lettuce seedlings have been exposed to TiO_2 and Ag nanoparticles and analyzed by inductively coupled plasma spectrometry, micro particle induced X-ray emission coupled to Rutherford backscattering spectroscopy on nuclear microprobe, micro X-ray fluorescence spectroscopy and X-ray absorption near edge structure spectroscopy. The benefits and drawbacks of each technique are discussed, and the type of information that can be drawn, for example on the translocation to edible parts, change of speciation within the plant, detoxification mechanisms, or impact on the plant ionome, are highlighted. Such type of coupled approach would be an asset for nanoparticle risk assessment.

Keywords: nanoparticle; micro X-ray fluorescence spectroscopy; X-ray absorption near edge spectroscopy; micro-particle induce X-ray emission/Rutherford backscattering spectroscopy; multivariate statistical analysis

1. Introduction

Nanotechnologies are developing fast with increasing number of applications in fields like medicine, sustainable development or plant protection products. They represent promising solutions to current issues such as more efficient disease treatment on targeted organs or decreased inputs of pesticides in the environment [1]. These new applications also imply an increased dissemination of nanoparticles (NPs, particles with at least one dimension below 100 nm) in ecosystems. Still, their fate in the environment is largely unknown mainly because of the lack of adapted techniques to assess their behavior in complex matrices (soil, plant or animal).

Two types of complementary techniques can be used to investigate the fate of NPs: bulk and imaging techniques. The most often used technique for the quantification of metallic NP on bulk samples is inductively coupled plasma – mass or atomic emission spectrometers (ICP-MS, ICP-AES) [7–9]. Although ICP techniques have very low detection limits (down to $ng.kg^{-1}$ [10]), and provide an essential information, they cannot provide spatial information. Thus, in the case of plant roots, they average adsorbed and absorbed elements from different tissue layers which can result in distorted data. Sample preparation can be an issue if proper acidic digestion of NPs has not been established. Often, standard digestion protocols do not take into account the particulate form of NPs, which may render them less soluble, and thus can lead to underestimation of NP content. Localizing NPs inside biological tissues requires 2D techniques such as scanning and transmission electron microscopy (SEM, TEM) coupled with an energy dispersive X-ray spectrometer (EDS) [2–4]. SEM is often used to investigate the fate of NPs on organism surface (for instance to visualize carbon nanotubes sticking out of root epidermis [5]) or on cross-sections but has a low sensitivity (detection limit around 1000 $mg.kg^{-1}$ [6]). TEM has a very good lateral resolution allowing investigations at the cellular to sub-cellular scale, but it is not suited for localization of metal at the organ scale. More important, sample preparation (water substitution, resin embedding, staining, coating) can generate artifacts and elemental relocalization. Existing cryotechniques (high pressure freezing, cryosubstitution) are highly valuable, but not commonly used in this field. These technical limitations represent a major bottleneck to advance our

understanding of NP fate in the environment.

To overcome these issues, the combination of both bulk analyses and 2D techniques is a powerful approach. In particular, micro beam-based techniques are useful but underused tools in biology [11–13]. These techniques are based on - but not restricted to - synchrotron radiation (photon) or ion (proton) beams. On synchrotron, elemental distribution can be studied by micro-X-ray fluorescence (μXRF) and chemical state by X-ray absorption near edge structure spectroscopy using a micro-focused beam (μXANES) or in full-field mode. On nuclear microprobes, metal distribution and *in situ* quantification can be obtained by combining micro-particle induced X-ray emission (μPIXE) and Rutherford backscattering spectroscopy (μRBS). These techniques are already well-known and widely used in chemistry, physics or material science but their development in biology and environmental sciences is more recent [12,13]. Latest developments in sample environment, detector sensitivity and spatial resolution had allowed their use for biological samples.

In this study, we report the complementarity of chosen beam-based techniques to determine the fate of two different types of NPs in a crop plant: lettuce (*Lactuca sativa*). Plants are a major component of ecosystems: they are at the interface between air, water and soil and at the base of the human food chain. We chose to study the behavior of two metal-containing NPs widely produced[1]: titanium dioxide (TiO_2) and silver (Ag) NPs. Moreover, these NPs have also been selected for their contrasted solubilities [14].

Lettuce seedlings were exposed in hydroponics to different concentrations of TiO_2 and Ag-NPs. After 7 days, plantlets were analyzed by a combination of techniques: ICP-MS and ICP-AES, μPIXE/RBS, μXRF and XANES. Emphasis has also been settled on sample preparation for the different techniques (optimization of the digestion procedure, preparation and observation of samples in cryogenic conditions). This innovative approach permitted to deepen our knowledge about NP fate in plants and to obtain original data about their impact on plant ionome.

2. Material and Methods

2.1. Plant culture & NP characterization

Lettuce seeds (*Lactuca sativa*, var. Laitue Romaine) were exposed for one week to 0, 10, 100, 1000 mg.L^{-1} Ag or TiO_2-NPs in a modified Hoagland solution. Those concentrations are representative of an acute contamination of the environment [15] and permitted to test the detection limits of the employed techniques. Uncoated Ag (≈ 40 nm) and TiO_2 (anatase, 4 nm) NPs were used. An Ag^+ exposure condition was also set-up to account for Ag-NP dissolution. More details on plant culture and NP characterization are available in the supplementary data and Figure S1 (Appendix).

2.2. Metal quantification by ICP-AES and ICP-MS

Usual digestion protocols (using hot HNO_3) might not be stringent enough to mineralize NPs as well as plant tissues, leading to the underestimation of metal concentrations. To obtain reliable data, effort was put to find out the best digestion protocol for both types of NPs testing the influence of several parameters (temperatures, type of acids, ratio NP powder/acid volume). Ag-NPs were easily mineralized regardless of the chemicals and the temperature conditions used. The following protocol, which was also efficient to mineralize plant tissue (white cabbage), was chosen: 1 mL HNO_3, 1.5 mL $HClO_4$ at 70°C during 24 h. For TiO_2-NPs, we chose a microwave assisted digestion using 5 ml H_2SO_4, 3 ml of HNO_3 and 1 ml of H_2O_2. Digestion yields of the different protocols are gathered in Table S1 (Appendix). Roots of three individuals per conditions were harvested, weighted and analysed for Ti and Ag concentrations on an ICP-AES for Ag-NPs and using an ICP-MS for TiO_2-NPs. More details are available in the supplementary data (Appendix).

2.3. Sample preparation for beam-based techniques

Beam-based techniques permit to have access to localized information. Sample preparation is a crucial step and if not properly done can lead to redistributions and changes in the speciation of elements [16]. To prevent this, samples were prepared under cryogenic conditions. First, roots and stems were thoroughly washed with deionized water to take off NPs lightly bound to the surface. Then samples

were cut in small pieces (2 mm) and immersed in a droplet of resin (Tissue Teck Sakura) and immediately cryo-fixed by plunging the sample in isopentane cooled with liquid nitrogen. The small size of the sample and droplet of resin allows rapid freezing of the whole tissue. Finally, samples were cut in thin cross-sections (20 µm) using a cryo-microtome (Leica). Cross-sections were mounted on appropriate sample holder for synchrotron experiments or freeze-dried (48h, -52°C, 0.01 mbars) for nuclear microprobe and XANES full-field analyses.

2.4. Proton beam-based techniques – *In situ* quantification by µPIXE/RBS

Samples (prepared as specified in 2.3) were analyzed in freeze-dried state under vacuum on the AIFIRA nuclear microprobe [17]. For this experiment, beamline was operated with a proton source at 3 MeV with a beam focused to 2.5 µm and a current intensity of 500 pA. Mapping of low-Z elements (H, C, N and O) was performed using RBS, in parallel with PIXE for the quantification of elements heavier than Mg. Detection limit is around 100 $\mu g.g^{-1}$. Data processing was performed using several softwares: Supavisio [18], SIMNRA [19] and GUPIX [20]. More details are available in the supplementary data (Appendix).

2.5. Synchrotron based techniques – Distribution by µXRF and chemical speciation by XANES

Synchrotron experiments were carried out on three beamlines: ID21 [21] and ID22 [22] at the European Synchrotron Radiation Facility (ESRF, Grenoble, France) and LUCIA at SOLEIL (Saint Aubain, France).

To avoid beam damage, acquisitions were performed under cryogenic conditions on ID21 and LUCIA.

µXRF maps were recorded with various step sizes (from 0.1 to 3 µm) with a dwell time from 100 to 2000 ms. µXRF data were fitted using PyMCA software [23].

Ag L_{III}-edge (3.33 to 3.45 keV energy range, 0.5 eV step) and Ti-K edge (4.96 to 5.05 keV energy range, 0.5 eV step) µXANES spectra were recorded in regions of interest of the fluorescence maps. The beam position was slightly moved from one spectrum to another to avoid radiation damage. At least 10

spectra of 30s were averaged for each point of interest, after checking the absence of radiation damage. XANES spectra on reference compounds were recorded during previous experiments [24,25] (Figure S2, Appendix).

Full-field measurements were performed at the ID21 XANES full-field end-station [26]. The achievable pixel size is 0.32 µm. Measurements were recorded on freeze-dried samples using the Si(111) monochromator with an energy step of 0.3 eV from 3.33 to 3.42 keV for Ag L-edge; and Si(220) with an energy step of 0.3 eV from 4.95 to 4.98 keV and 1 eV from 4.98 to 5.06 keV for Ti K-edge. Data processing was made using the SIFT_PyOCL procedure [27] and TXM-Wizard [28].

XANES data treatment was performed using Athena software [29] according to Larue *et al*. [24,25].

More details are available in the supplementary data (Appendix).

2.6. Statistical analysis

To achieve normality and homoscedasticity, data were $\log_{10}$ transformed. They were compared using one-way ANOVA (for Ti and Ag concentrations in roots as measured by ICP) or two-way ANOVA (for plant fresh biomass), with organ (roots or leaves) and treatment (control, TiO_2-NPs, Ag ionic and Ag-NPs) as main effects, and the interaction (organ x treatment). Post hoc tests (pairwise T-tests with Bonferroni correction, and Tukey tests) were applied to detect differences between groups of samples. Differences were considered significant when $p \leq 0.05$.

To analyze µPIXE/RBS quantitative results and the effect of the different NP concentrations on the root (divided in epidermis, parenchyma and vascular cylinder) ionome (comprising Ca, Cl, Cu, Fe, K, Mn, Mg, Na, P, S, Si and Zn concentrations) we used linear discriminant analysis (LDA) and principal component analysis (PCA). Those techniques are known as part of a group of exploratory data analyses which permit to accommodate the small number of biological replicates due to beamtime restrictions. Data were first $\log_{10(+1)}$ transformed, then standardized. For LDA, the homogeneity between within-group covariance matrices were tested *prior* the analysis.

All statistical analyses were performed using the R statistical software [30], with the vegan [31] and MASS [32] packages.

3. RESULTS and DISCUSSION

3.1. Toxicity symptoms and ICP metal concentrations

Exposure to the highest NP concentration (1000 $mg.L^{-1}$) affected the plant fresh weight (F=3.48, P=0.041), but no interaction between NP treatment and organs could be detected (F=0.90, P=0.46), indicating that both roots and leaves were affected similarly by the exposure to NPs (Figure S3A, Appendix). Plants showed reduced fresh weight in roots and leaves when exposed to Ag-NPs (roots: 176.60 ± 78.78 mg; leaves: 1165.87 ± 350.73 mg) and Ag^+ (roots: 150.97 ± 54.30 mg; leaves: 1172.70 ± 625.73 mg) in comparison to control (roots: 349.83 ± 121.82 mg; leaves: 1312.70 ± 328.77 mg) and TiO_2-NP treated plants (roots: 322.67 ± 95.54 mg; leaves: 1586.63 ± 433.67 mg). Plants exposed to Ag (ions and NPs) were displaying early senescence signs and brownish roots (Figure S3B, Appendix).

These results are consistent with previous studies on various plants reporting no acute phytotoxicity symptoms following TiO_2-NP exposure [33–37] but decreased root length and biomass after Ag-NP treatment for rice [38] or ryegrass [39]. A study published on the comparative effect of Ag-NPs *vs.* TiO_2-NPs on tomato also highlighted different phytotoxicity profiles [40]. It is also interesting to notice that the condition accounting for Ag-NP dissolution led to the same growth inhibition that the Ag-NP condition itself. It brings to light the usual question dealing with Ag-NP toxicity: does it come from the NPs or from the dissolution of Ag^+ ions? According to several studies Ag as ions would be more toxic than Ag as NPs [41–43]. However, NP toxicity would come for a large part from the release of Ag ions during exposure but the nanoparticulate form would also play a specific role in the phytotoxicity process: negatively charged NPs might diffuse more easily than cations within organic matrices [43], and internalized Ag-NPs might then release Ag^+ inside the biological compartments [44–46]. Within the framework of our experiment (high Ag concentrations, short-term exposure), our results rather

support the hypothesis of toxicity coming primarily from Ag ions. This conclusion is in good agreement with a study showing that, if the soluble Ag fraction is high, NPs will not add measurable additional toxicity but at low Ag ionic fraction the nanoparticulate form will increase the phytotoxicity [44].

After exposure, metal concentrations in plants were assessed by ICP-AES and ICP-MS. Roots of control seedlings contained low level of both metals (Ti and Ag < 6 $mg.kg^{-1}$). After a 7-day exposure to 1000 $mg.L^{-1}$ NPs, it was significantly higher: 238.0 ± 54.9 ($F=128.2$, $P=1.2.10^{-5}$) and 1600.5 ± 271.3 ($F=49.42$, $P=0.002$) $mg.kg^{-1}$ fresh weight (FW) of Ag and Ti respectively (Figure S4, Appendix).

Ti root concentration was more than 6 times higher than Ag root concentration when exposed to the same initial NP concentration. This trend was not seen in the other comparative study between Ag and TiO_2-NPs on tomato in which Ag concentration in roots was higher [40]. This difference could be linked to the difference in exposure media. Tomato seedlings were exposed in ultrapure water and lettuces in this study in Hoagland solution; this will impact NP behaviour in suspension (agglomeration and dissolution) and thus their interaction with plants. Moreover, different species might also have different uptake as suggested by a study comparing Ti uptake in wheat, common bean and curly dock [34] showing root concentration ranging from 2460 to 5280 $mg.kg^{-1}$. Additionally, no information is available on the digestion protocol used for ICP measurements so direct comparison might not be pertinent (Table S1, Appendix). Another interesting fact is that the same growth inhibition of the two Ag treatments noticed before (Figure S3, Appendix) is not linked to similar Ag concentrations in lettuce roots. Ag concentration in roots of seedlings exposed to Ag^+ was significantly lower (82.3 ± 5.2 $mg.kg^{-1}$ FW, $F=128.2$, $p=1.2.10^{-5}$) than in plants exposed to Ag-NPs (Figure S3A, Appendix). This result suggests that not only Ag^+ ions first dissolved from NPs in the medium are taken up by lettuce roots. Several hypotheses can be proposed: (i) either NPs can penetrate plant roots creating “channels” (as it has been suggested for carbon nanotubes and tomato seed coat [47]) that will facilitate other ion/NP internalisation and internalized NPs would release ions directly into cells [46], or (ii) NP interaction with the root surface enhances their dissolution at the vicinity of the root and subsequently the uptake

of Ag^+ [39,42] with possible later Ag reduction inside organisms [48], or (iii) a large part of NPs and their secondary products are sorbed on the root surface.

Finally, these ICP measurements suggest that there is no apparent link between toxicity symptoms (more toxicity for Ag) and metal accumulation in roots (more Ti accumulated).

However, ICP-AES and ICP-MS provide bulk analyses and do not distinguish between metal adsorbed on the root surface *vs*. internalized inside the roots. To shed light on this aspect, a spatially resolved and quantitative approach is needed.

3.2. *In situ* quantification by µPIXE/RBS

Lettuce roots were exposed to Ag^+ (10 $mg.L^{-1}$), Ag-NPs and TiO_2-NPs (10 to 1000 $mg.L^{-1}$); root and stem cross-sections were imaged by µPIXE (Figure S5 - Appendix, Table 1). The Ag^+ treatment lead to undetectable level of Ag using this technique and was discarded from the analysis. µRBS analysis in parallel made it possible to obtain reliable local quantification by area of interest in the samples (Figure S5, S6 - Appendix). Differently to ICP-AES/ICP-MS analyses, results are expressed in $mg.kg^{-1}$ dry weight (DW). For rough estimation, one could consider 10% of dry matter for lettuce roots.

Considering results averaged on the whole cross-section including the root surface, µPIXE/RBS and ICP-AES/ICP-MS results are in good agreement, evidencing a different behavior between the TiO_2 and Ag NPs (Figure S6, Appendix). In the analyzed cross-sections, Ti was 12 times more concentrated than Ag: 25390 and 2096 $mg.kg^{-1}$ DW respectively after the 1000 $mg.L^{-1}$ treatment. The difference between Ti and Ag concentration at the cross-section scale is due to a high Ti adsorption on root epidermis in comparison with the parenchymal concentration (for Ti $p<0.05$, for Ag $p=0.26$): 71455 ± 10083 mg $Ti.kg^{-1}$ in the epidermis area vs. 5888 ± 5670 mg $Ag.kg^{-1}$. So using a 2D mapping technique and focusing on the contribution of each tissue type (epidermis *vs*. parenchyma *vs*. vascular cylinder), the conclusion is different. If the epidermis area is discarded, one can conclude that lettuce root had taken up more Ag than Ti with approximately 878 ± 399 mg $Ag.kg^{-1}$ DW contained in the parenchyma and vascular cylinder compared to 99 ± 89 $mg.kg^{-1}$ DW for Ti (Figure S6, Appendix). This phenomenon was also

suggested to explain the high Ti concentration in *Vicia faba* [35], bean [34], wheat [34,36] and rapeseed [37]. In terms of risk assessment, these µPIXE/RBS results suggest that Ag is more worrying since it is taken up by lettuce roots in higher amount and thus is more susceptible to translocate towards the edible parts. Inversely, Ti is found aggregated at the root surface but a small amount is internalized. If one had only considered ICP-AES/ICP-MS data, the conclusion would have been the reverse.

The leaves were not analyzed by ICP-AES, but stem cross-sections for the plants exposed to 1000 $mg.L^{-1}$ were analyzed by µPIXE to identify a possible translocation of Ag and Ti towards the leaves (Figure S6, Appendix). Ti was detected in all stem tissues: epidermis: 283 ± 292 $mg.kg^{-1}$, parenchyma: 27 ± 15 $mg.kg^{-1}$ and vascular cylinder: 48 ± 39 $mg.kg^{-1}$. Its distribution was uneven with for instance a hot spot of Ti in the stem vascular cylinder at 2254 $mg.kg^{-1}$ DW and high variations within replicates. Ag was not detected in the stem even if its concentration in roots was higher than Ti concentration. An explanation to this phenomenon could be the chemical form of the detected element. If Ag is dissolved inside plants then Ag ions would be more mobile and distributed homogeneously in plant tissue leading to a low local Ag concentration, below detection limit. Inversely, Ti due to its limited dissolution would remain as NPs and form hot spots of aggregated NPs thus reaching locally the detection limit of µPIXE technique.

To evaluate the most appropriate exposure condition for this type of experiment, plants were also exposed to 10 and 100 $mg.L^{-1}$ TiO_2 and Ag-NPs. At 100 $mg.L^{-1}$ Ag was still detectable in the parenchyma of lettuce roots with approximately the same concentrations as when exposed to 1000 $mg.L^{-1}$ but was under detection limits in the vascular cylinder. At the lowest exposure concentration (10 $mg.L^{-1}$), Ag was always below detection limits. Inversely, Ti was detectable in all used concentrations with the existence of Ti overaccumulation on root epidermis. This comparison with lower concentrations confirms results obtained at the highest concentration and also validates our hypothesis of the lower detectability of Ag in comparison to Ti. Even if Ag is more taken up by lettuce than Ti, it becomes under detection limit for lower doses whereas Ti is still detectable.

Interestingly, there was no significant difference in Ti concentrations between the 100 and the 1000 mg.L^{-1} treatments (p=0.96). This can be explained by the higher accumulation of Ti at the root surface in the 1000 mg.L^{-1} exposure which might act as a physical barrier limiting the diffusion and uptake of Ti inside the root tissues (lower Ti concentration in both the parenchyma and vascular cylinder). This effect was not visible for Ag-NP exposure in which concentrations in the tissues increased with Ag exposure ($p=5.73.10^{-9}$).

A question arising from the high accumulation of Ti on the root surface is its potential influence on plant ionome [49]. Very little has been done so far to investigate the impact of NP exposure on plant nutrition (*Elodea Canadensis* [34], *Arabidopsis thaliana* [50]) and presently there is no study on crop plants. A major advantage of µPIXE is the possibility to access the distribution of all elements permitting the identification of co-localizations or changes in elemental concentrations.

To analyze the effect of different NP concentrations on the elemental accumulation in roots, we used multivariate statistics analysis techniques, namely LDA and PCA. Both techniques are widely used in multivariate statistics [51], LDA being applied to discriminate classes of data, and PCA to identify relationships between variables, without taking into account classes or structures in the data. Across all conditions (NP concentrations and plant tissues), a clear discrimination (LD1: 0.8086) between the control and NP-exposed roots could be detected by LDA (Figure 1A), with Cu (eigenvalue=2.53, Ctl: 202 mg.kg^{-1}, Ag-NP: 39 mg.kg^{-1}, TiO_2-NP: 42 mg.kg^{-1}), Fe (eigenvalue=-1.96, Ctl: 22 mg.kg^{-1}, Ag-NP: 38 mg.kg^{-1}, TiO_2-NP: 40 mg.kg^{-1}), Mn (eigenvalue=1.50, Ctrl: 195 mg.kg^{-1}, Ag-NP: 25 mg.kg^{-1}, TiO_2-NP: 59 mg.kg^{-1}) and Ca (eigenvalue=-1.30, Ctrl: 9923 mg.kg^{-1} , Ag-NP: 22374 mg.kg^{-1}, TiO_2-NP: 213482 mg.kg^{-1}) being among the most important elements for the discrimination of the groups on the first discriminant axis. A less clear discrimination between the Ag and TiO_2 treatments could be detected (as seen by the partial overlap of the 90% tolerance intervals in Figure 1A), indicating a possible common effect of both NPs on the root elemental concentrations. ICP measurements on Arabidopsis exposed to Ag-NPs showed a decreased concentration for K, Fe and Zn [50]. Though the direct comparison is difficult because of the very different exposure conditions (2 mg.L^{-1} in agar medium *vs*. 10 to 1000 mg.L^{-1} in

hydroponics), LDA on lettuce roots also highlighted a disrupted Fe homeostasis with an eigen value of -1.96 whereas the two other elements (K and Zn) were not modified which suggest a species-dependent effect.

To gain deeper insights on the effects of the different NPs and the relationships between elements, a PCA was performed (Figure 1B). Overall, exposure to Ag-NPs led to a decrease in the concentration of several elements (such as Cu, Zn, Mn, P, S and K) indicating a large disruption of the root ionome, whereas common effect of Ag-NPs and TiO_2-NPs could be seen but only when plants were exposed to 1000 $mg.L^{-1}$. The highest concentration of TiO_2-NPs also led to a higher accumulation of Fe, P, S and Ca in the root epidermis, not seen at the lower concentrations. Those higher concentrations in the epidermis are correlated with decreased concentrations in both the parenchyma and vascular cylinder of plants treated with 1000 $mg.L^{-1}$ TiO_2-NPs, leading to a similar profile as to plants exposed to Ag-NPs. The same analyses were also performed after excluding the epidermis from the data set, to consider only the internal tissues (Figure S7A, B - Appendix). They provided the same clustering of data, and led to the same conclusions on the changes in root ionome.

Figure 1. Root ionome analyzed by µPIXE/RBS. A. LDA statistical analysis of elemental concentrations in roots. B. PCA statistical analysis of elemental concentrations in roots. Elements included in the analysis are Na, Mg, Si, P, Cl, K, Ca, Mn, Fe, Cu and Zn (Ti and Ag excluded). For the figure in color, the reader is referred to the web version of this article.

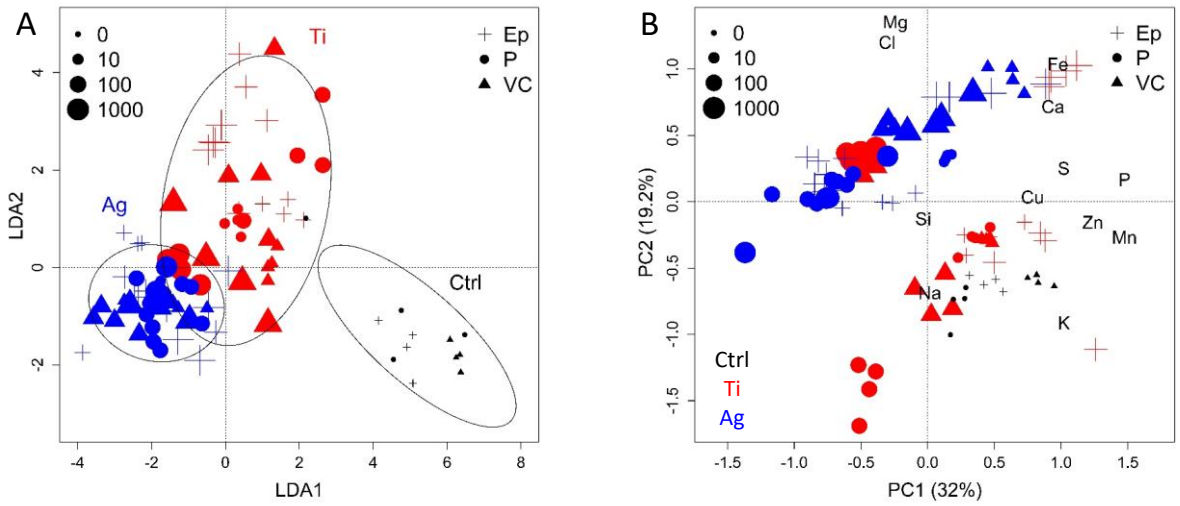

325

326

327 To conclude, µPIXE/RBS experiment evidenced a similar impact of Ag-NPs on plant ionome at all
328 exposure concentrations, whereas TiO_2-NPs displayed a different impact at very high concentration
329 (1000 $mg.L^{-1}$) as compared to lower concentrations (<100 $mg.L^{-1}$). Even without visible acute toxicity
330 symptoms at one week exposure, high concentrations of TiO_2-NPs may lead to a long-term toxicity by
331 acting as a physical barrier disrupting plant homeostasis.

332

333 **3.3. Metal speciation by XANES**

334 To investigate the influence of metal chemical form in plants on their fate, metal speciation *in situ* was
335 determined by XANES. To perform µXANES *in situ*, elemental distribution was first mapped by
336 synchrotron radiation based-µXRF (Table 1). The detection limit of µXRF is lower than for µPIXE, around
337 1 $µg.g^{-1}$ in the tissues [52]. The limit to assure a good XANES data quality is one or two orders of
338 magnitude higher. Thus, the highest exposure condition was chosen for synchrotron experiments
339 (1000 $mg.L^{-1}$ in the exposure medium). Distribution maps of metals in root and stem cross-sections
340 obtained after exposure to 1000 mg TiO_2-NPs.L^{-1} and 1000 mg Ag-NPs.L^{-1} are presented in Figure 2.
341 µXRF results agreed with µPIXE results, showing a continuous layer of Ti at the root surface associated
342 with Ca and P (Figure 2E, F, G, H) which explains the high contribution of Ca and P on the PC1 of the
343 previous PCA analysis (Figure 1B). Likewise, hot spots of Ti were detected inside roots, in the

parenchyma and in the stem (Figure 2E, F). Ag appeared as agglomerates on root epidermis (Figure 2A, B). Moreover, the high sensitivity of µXRF also permitted to detect Ag in the root vascular bundle (Figure 2C, D) as well as in vascular bundles in the stem (Figure 2I, J, K, L). The presence of Ag in the root vascular cylinder was further confirmed by µXRF analysis of a freeze-dried root cross-section at the hard X-ray nanoprobe beamline ID22 (excitation at 29.5 KeV, above Ag K-edge) (Table 1, Figure S8A, B – Appendix). Exciting above the Ag K-edge enhances the sensitivity for Ag due to the higher fluorescence yield of the K emission lines together with the higher photon flux provided at this beamline. However at this high energy other relevant elements such S, P, Cl, K and Ca are poorly detected. These data support the hypothesis that Ag-NPs were transferred through the vascular system to the edible tissue of lettuces. For TiO_2-NPs the conclusion needs to be mitigated since this Ti also exists as a geogenic element in earth crust. Translocation of both TiO_2 and Ag-NPs in other plant species and transfer to edible parts of crops including cucumber [53,54], tomato [40] and rice [38] have already been demonstrated.

Figure 2. µXRF analysis of lettuce roots and stems exposed for 7 days in hydroponics to 1000 mg.L^{-1} Ag-NPs or 1000 mg.L^{-1} TiO_2-NPs. Two color maps show Ag (A, C, I, K) or Ti (E, M) (red) superimposed to endogenous elements (S, P, K or Cl in green). Elemental distribution maps in temperature color for Ag (B, D, J, L), Ti (F, N), P (G) and Ca (H). Color bars represent the fluorescence counts. Maps were acquired on ID21 and LUCIA. Arrows indicate spots where µXANES spectra were recorded. For the figure in color, the reader is referred to the web version of this article.

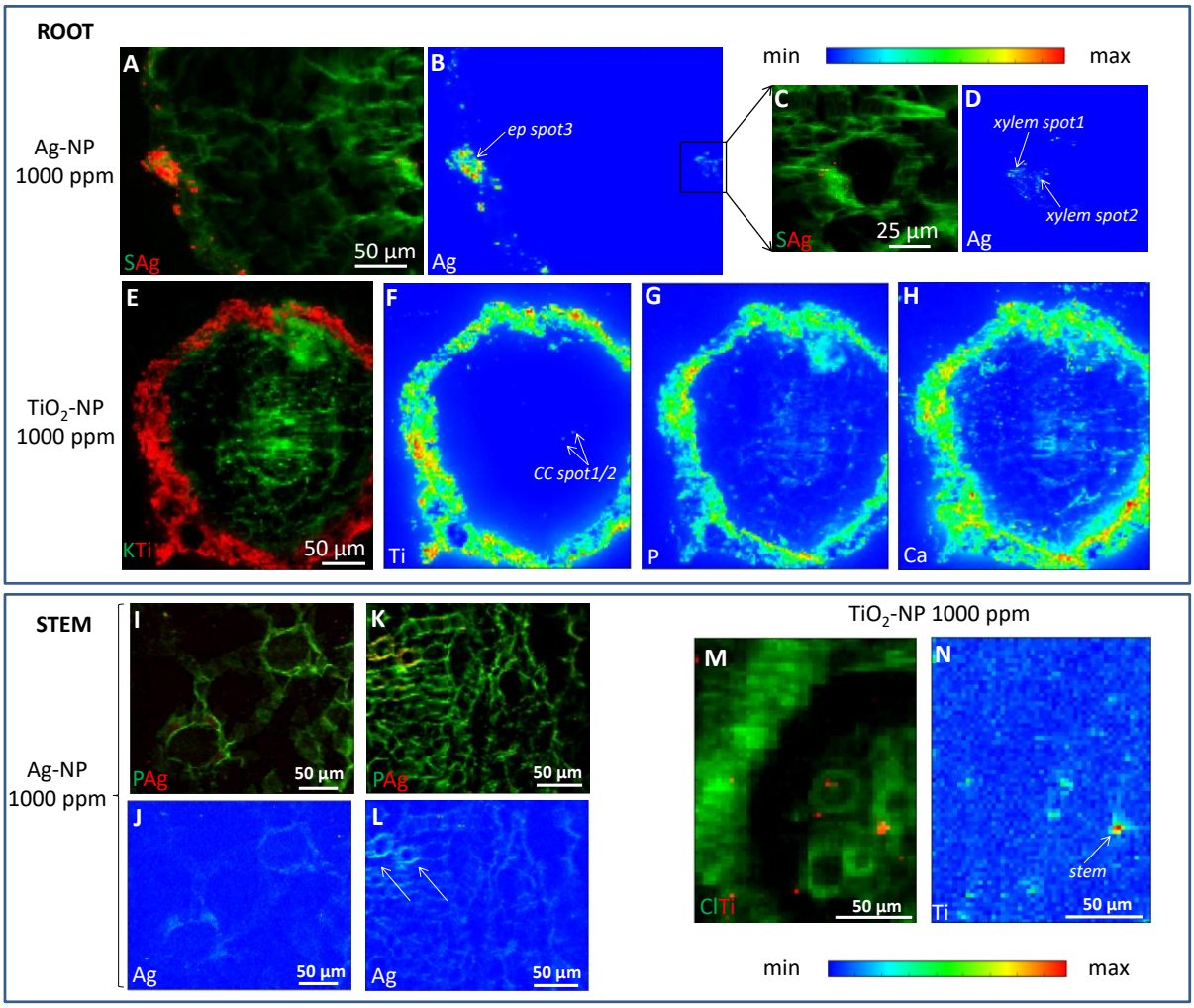

Metal speciation was determined from these maps (arrows in Figure 2 and data not shown) by µXANES and using linear combination fitting of reference compounds (Table 1). Ti in the epidermis as well as in the root parenchyma and vascular cylinder was present as anatase. It was also transferred to stems in this chemical state (Figure 3A, Figure S9A, B - Appendix). The stability of anatase NPs in the plants is consistent with previous publications [36,37,53,54]. Inversely, Ag was present in roots under two oxidation states from 100% Ag^0 to 100% monovalent Ag and in association with different ligands regardless of the tissue (Figure 3B). The predominant ligand identified by linear combination fitting is a thiol-containing molecule (glutathione). This molecule is known to be involved in plant detoxification mechanisms and has been shown to increase in concentration in wheat exposed to Ag-NPs [55]. Ag-thiol complexes have already been detected in lettuce leaves after foliar exposure to Ag-NPs [24]. Ag

in leaves was too diluted to obtain exploitable XANES spectra. Likewise, no good quality XANES spectra could be obtained for roots exposed to lower NP concentrations (10 and 100 mg.L^{-1}).

Figure 3. XANES analysis in situ of Ti and Ag in root (VC: root vascular cylinder, par: root parenchyma, ep: root epidermis) and stem cross-sections of lettuce in different acquisition modes: µXANES (Ti in A and Ag in B) and in XANES full-field mode (transmission map of a root cross-section in C with selected area for XANES extraction, corresponding spectra in D. "total" corresponds to all extractible spectra of the analyzed area). In plain lines experimental data, in dotted lines the fit and reference compound contributions to the linear combination fits. For the figure in color, the reader is referred to the web version of this article.

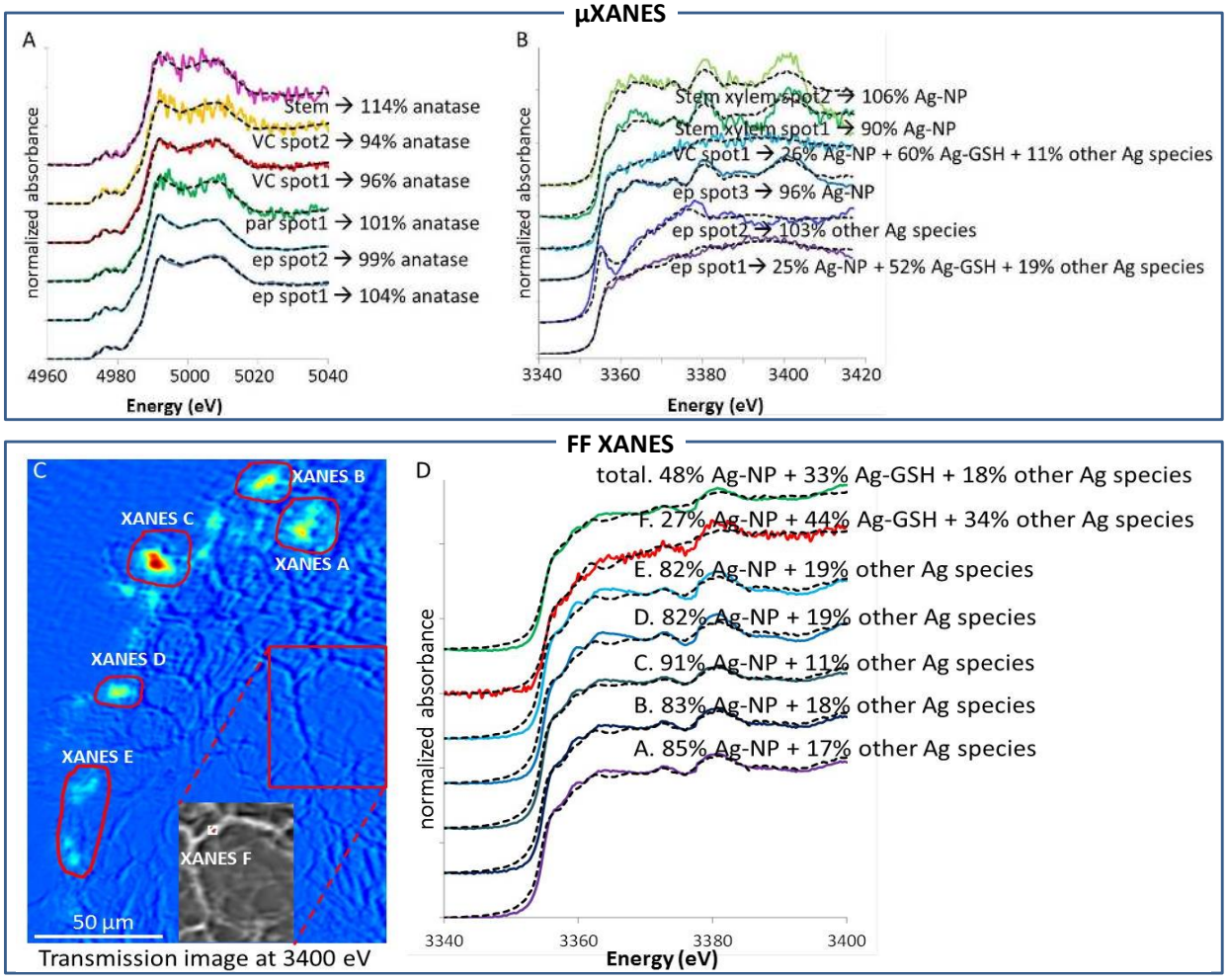

To have a better understanding of Ag internalization mechanisms, a root cross-section was analyzed by full-field XANES (Figure 3C, D, Table 1). This technique permits to obtain 2D speciation of an element

of interest over a large area but is restricted to samples with high concentrations of this element and to thin cross-sections since the signal is recorded in transmission mode. At the moment this acquisition mode runs at room temperature only, so root cross-sections were freeze-dried before analysis. The overall signal of the root cross-section showed a contribution of three forms of Ag, half of the signal came from Ag-NPs, and the other half from other Ag species with 33% being complexed by a thiol-containing molecule. A spatial segregation seemed to exist between the epidermis and the parenchyma. Indeed, Ag at the root surface showed only a moderate dissolution (between 10 and 20%) whereas Ag in the parenchyma displayed a higher dissolution (78%, XANES F). These speciation results corroborate the hypothesis stated after µPIXE/RBS analysis: Ag inside root tissue was mainly present as monovalent Ag, with a small contribution from elemental Ag (as Ag-NPs). These results do not permit to distinguish the two internalization scenarios stated before: only ions are internalized *vs.* Ag-NPs are internalized and dissolved inside the cells. Indeed, plant exposure to ionic Ag also led to the formation of Ag^0 in plant tissues [24,56,57]. Since TiO_2-NPs can be internalized, it is conceivable that Ag-NPs are internalized as well. Thus, the two pathways probably co-exist: both Ag ions and Ag-NPs are taken up by roots, with later dissolution of Ag-NPs inside the tissue and resulting Ag^+ ions are partly scavenged by the detoxification system. XANES analysis confirmed different behaviors for the two NPs: Ti was detected in plant tissues as agglomerated but unchanged NPs, unlike Ag which was present as Ag-NPs and secondary species including Ag^+ bound to thiol ligands.

Table 1: Summary of spectroscopic techniques employed in this study

Technique	Instrument	Information	Characteristics
µXRF	Synchrotron (ID21 and LUCIA)	Distribution at the Ti K and Ag L edge	Very sensitive (1 $\mu g.g^{-1}$) In association with µXANES Cryogenic conditions
µXRF	Synchrotron (ID22*)	Distribution at Ag K edge	K-edge more sensitive Better lateral resolution (sub-cellular scale) No information on light elements Freeze-dried samples
µXANES	Synchrotron (ID21)	Speciation	*in situ* Cryogenic

Full-field XANES	Synchrotron (ID21)	Speciation	*in situ* Fast acquisition on large area Concentrated and thin samples (in transmission) Freeze-dried samples
µPIXE/RBS	nuclear microprobe (AIFIRA)	Distribution + quantification	Sensitivity (100 µg.g^{-1}) Local quantification For all elements (H→U) Freeze-dried samples

410 ** Since our experiment, ID22 nanoimaging beamline has been upgraded and relocated at ID16 (NINA).*

411

412 **Conclusion**

413 This study highlights the interest of using spectroscopic beam-based techniques to analyze the fate of
414 NPs in the environment and especially in biological matrixes. It permitted to bring new and original
415 information that are mandatory for understanding the fate of NPs in plants, which are key information
416 for risk assessment and food safety. For instance, µPIXE/RBS and µXRF showed that Ag-NPs were more
417 efficiently taken up by roots than TiO_2-NPs, whereas considering only ICP-MS/AES data, one could have
418 had a reverse conclusion because of the presence of TiO_2-NPs adsorbed on the root surface. Ag and Ti
419 were observed in the stem, suggesting a transfer of the NPs and/or their secondary products to the
420 edible parts of lettuce. The study of the speciation by XANES demonstrated different behaviors for
421 those two NPs: Ti was detected in root tissues as agglomerated but unchanged NPs, unlike Ag which
422 was present as Ag-NPs and secondary species including Ag^+ bound to thiol ligands. Another interesting
423 piece of information is related to NP toxicity. In our exposure conditions, TiO_2-NPs were not acutely
424 toxic however, at high concentrations they had a clear impact on root homeostasis by disrupting Fe,
425 Ca and P uptake which may lead to long-term toxicity. On the other hand, Ag-NPs were phytotoxic at
426 all concentrations tested and altered to a higher extent root ionome. Obviously, those results have to
427 be mitigated since exposure conditions are not representative of chronic contaminations. This
428 represents the main limit of those techniques nowadays: their limit of detection which restricted, until
429 recently, studies to exposure concentrations mimicking an acute contamination of the environment.
430 Many other spectroscopic techniques exist that are equally useful and bring complementary data for
431 instance at the sub-cellular level (nanoSIMS) or in depth profiling (ToF-SIMS) or on the bio-

macromolecule distribution (μFTIR). Finally coupling those spectroscopic methods with biochemical and molecular information would be a very powerful and promising approach in the future.

ACKNOWLEDGEMENTS

The authors would like to thank the FP7 of the European Union for the funding (Nanohouse project no. 247810), the French program Equipex NanoID (ANR-10-EQPX-39-01), and French program LABEX Serenade (11-LABX-0064). Synchrotron experiments were performed on ID21 and ID22 beamlines at the European Synchrotron Radiation Facility (ESRF), Grenoble, France and on LUCIA beamline at SOLEIL (St Aubin, France). ISTerre is part of Labex OSUG@2020 (ANR10 LABX56). AIFIRA nuclear microprobe is also acknowledged for beamtime provision. The authors would like to thank Dr. Antoine Gehin for his precious help to prepare reference compounds in anoxic conditions for XANES experiment. The authors declare no competing financial interest.

APPENDIX A. SUPPLEMENTARY DATA

Supplementary data to this article can be found online at doi:

448 **BIBLIOGRAPHY**

449 [1] www.nanotechproject.org, The project on emerging nanotechnologies, (2015).
450 [2] C. Kole, P. Kole, K.M. Randunu, P. Choudhary, R. Podila, P.C. Ke, et al., Nanobiotechnology can
451 boost crop production and quality: first evidence from increased plant biomass, fruit yield and
452 phytomedicine content in bitter melon (Momordica charantia), BMC Biotechnol. 13 (2013) 37–
453 47. doi:10.1186/1472-6750-13-37.
454 [3] A. Massarsky, R. Abraham, K.C. Nguyen, P. Rippstein, A.F. Tayabali, V.L. Trudeau, et al.,
455 Nanosilver cytotoxicity in rainbow trout (Oncorhynchus mykiss) erythrocytes and hepatocytes,
456 Comp. Biochem. Physiol. Part C Toxicol. Pharmacol. 159 (2014) 10–21.
457 doi:10.1016/j.cbpc.2013.09.008.
458 [4] S. Li, L.K. Wallis, H. Ma, S.A. Diamond, Phototoxicity of TiO(2) nanoparticles to a freshwater
459 benthic amphipod: are benthic systems at risk?, Sci Total Env. 466-467 (2014) 800–808.
460 doi:10.1016/j.scitotenv.2013.07.059.
461 [5] C. Larue, M. Pinault, B. Czarny, D. Georgin, D. Jaillard, N. Bendiab, et al., Quantitative evaluation
462 of multi-walled carbon nanotube uptake in wheat and rapeseed, J. Hazard. Mater. 227 (2012)
463 155–163. doi:10.1016/j.jhazmat.2012.05.033.
464 [6] J. Goldstein, D. Newbury, D. Joy, C. Lyman, P. Echlin, E. Lifshin, et al., Scanning Electron
465 Microscopy and X-ray Microanalysis, Springer, 2003.
466 [7] E. Bigorgne, L. Foucaud, E. Lapied, J. Labille, C. Botta, C. Sirguey, et al., Ecotoxicological
467 assessment of TiO2 byproducts on the earthworm Eisenia fetida, Env. Pollut. 159 (2011) 2698–
468 2705. doi:10.1016/j.envpol.2011.05.024.
469 [8] D. Cleveland, S.E. Long, P.L. Pennington, E. Cooper, M.H. Fulton, G.I. Scott, et al., Pilot estuarine
470 mesocosm study on the environmental fate of silver nanomaterials leached from consumer
471 products, Sci Total Env. 421-422 (2012) 267–272. doi:10.1016/j.scitotenv.2012.01.025.
472 [9] R. Kaveh, Y.S. Li, S. Ranjbar, R. Tehrani, C.L. Brueck, B. Van Aken, Changes in Arabidopsis
473 thaliana gene expression in response to silver nanoparticles and silver ions, Env. Sci Technol. 47
474 (2013) 10637–10644. doi:10.1021/es402209w.
475 [10] C. Mariet, O. Belhadj, S. Leroy, F. Carrot, N. Metrich, Relevance of NH4F in acid digestion before
476 ICP-MS analysis, Talanta. 77 (2008) 445–450.
477 [11] E. Donner, T. Punshon, M.L. Guerinot, E. Lombi, Functional characterisation of metal(loid)
478 processes in planta through the integration of synchrotron techniques and plant molecular
479 biology, Anal. Bioanal. Chem. 402 (2012) 3287–3298. doi:10.1007/s00216-011-5624-9.
480 [12] G. Sarret, E. Pilon-Smits, H. Castillo-Michel, M. Isaure, F.J. Zhao, R. Tappero, Use of synchrotron-
481 based techniques to elucidate metal uptake and metabolism in plants, in: D.L. Sparks (Ed.), Adv.
482 Agonomy, Academic Press, 2013: pp. 1–82.
483 [13] B. Wang, Z. Wang, W. Feng, M. Wang, Z. Hu, Z. Chai, et al., New methods for nanotoxicology:
484 synchrotron radiation-based techniques, Anal. Bioanal. Chem. 398 (2010) 667–676.
485 doi:10.1007/s00216-010-3752-2.
486 [14] G.E. Schaumann, A. Philippe, M. Bundschuh, G. Metreveli, S. Klitzke, D. Rakcheev, et al.,
487 Understanding the fate and biological effects of Ag- and TiO2-nanoparticles in the environment:
488 The quest for advanced analytics and interdisciplinary concepts, Sci. Total Environ. 535 (2014)
489 3–19. doi:10.1016/j.scitotenv.2014.10.035.
490 [15] A. Gogos, K. Knauer, T.D. Bucheli, Nanomaterials in plant protection and fertilization: current
491 state, foreseen applications, and research priorities, J. Agric. Food Chem. 60 (2012) 9781–9792.
492 doi:10.1021/jf302154y.
493 [16] A.G. Kachenko, R. Siegele, N.P. Bhatia, B. Singh, M. Ionescu, Evaluation of specimen preparation
494 techniques for micro-PIXE localisation of elements in hyperaccumulating plants, Nucl. Instrum.
495 Methods Phys. Res. Sect. B Beam Interact. Mater. At. 266 (2008) 1598–1604.
496 doi:10.1016/j.nimb.2007.11.017.

[17] S. Sorieul, P. Alfaurt, L. Daudin, L. Serani, P. Moretto, Aifira: An ion beam facility for multidisciplinary research, Nucl. Instrum. Methods Phys. Res. Sect. B Beam Interact. Mater. At. 332 (2014) 68–73. doi:10.1016/j.nimb.2014.02.032.
[18] BARBOTTEAU Software Informer: Latest BARBOTTEAU software updates and reviews: SupaVISIO, etc., (n.d.). http://barbotteau.software.informer.com/ (accessed September 28, 2015).
[19] M. Mayer, SIMNRA, a simulation program for the analysis of NRA, RBS and ERDA, in: J.L. Duggan, I.L. Morgan (Eds.), Appl. Accel. Res. Ind. Pts 1 2, Amer Inst Physics, Melville, 1999: pp. 541–544. ://000081503200132.
[20] J.L. Campbell, T.L. Hopman, J.A. Maxwell, Z. Nejedly, The Guelph PIXE software package III: Alternative proton database, Nucl. Instrum. Methods Phys. Res. Sect. B-Beam Interact. Mater. At. 170 (2000) 193–204. doi:10.1016/S0168-583X(00)00156-7.
[21] M. Salomé, M. Cotte, R. Baker, R. Barrett, N. Benseny-Cases, G. Berruyer, et al., The ID21 Scanning X-ray Microscope at ESRF, J. Phys. Conf. Ser. 425 (2013) 182004.
[22] G. Martínez-Criado, R. Tucoulou, P. Cloetens, P. Bleuet, S. Bohic, J. Cauzid, et al., Status of the hard X-ray microprobe beamline ID22 of the European Synchrotron Radiation Facility, J. Synchrotron Radiat. 19 (2012) 10–18. doi:10.1107/S090904951104249X.
[23] V.A. Sole, E. Papillon, M. Cotte, P. Walter, J. Susini, A multiplatform code for the analysis of energy-dispersive X-ray fluorescence spectra, Spectrochim. Acta Part B-At. Spectrosc. 62 (2007) 63–68. doi:10.1016/j.sab.2006.12.002.
[24] C. Larue, H. Castillo-Michel, S. Sobanska, L. Cécillon, S. Bureau, V. Barthès, et al., Foliar exposure of the crop Lactuca sativa to silver nanoparticles: Evidence for internalization and changes in Ag speciation, J. Hazard. Mater. 264 (2014) 98–106. doi:10.1016/j.jhazmat.2013.10.053.
[25] C. Larue, H. Castillo-Michel, S. Sobanska, N. Trcera, S. Sorieul, L. Cecillon, et al., Fate of pristine TiO2 nanoparticles and aged paint-containing TiO2 nanoparticles in lettuce crop after foliar exposure, J Hazard Mater. 273 (2014) 17–26. doi:10.1016/j.jhazmat.2014.03.014.
[26] B. Fayard, E. Pouyet, G. Berruyer, D. Bugnazet, C. Cornu, M. Cotte, et al., The new ID21 XANES full-field end-station at ESRF, J. Phys. Conf. Ser. 425 (2013) 192001.
[27] P. Paleo, E. Pouyet, J. Kieffer, Image stack alignment in full-field X-ray absorption spectroscopy using SIFT_PyOCL, J. Synchrotron Radiat. 21 (2014) 456–461. doi:10.1107/S160057751400023X.
[28] Y. Liu, F. Meirer, P.A. Williams, J. Wang, J.C. Andrews, P. Pianetta, TXM-Wizard: a program for advanced data collection and evaluation in full-field transmission X-ray microscopy, J. Synchrotron Radiat. 19 (2012) 281–287. doi:10.1107/S0909049511049144.
[29] Ravel, Newville, ATHENA, ARTEMIS, HEPHAESTUS: data analysis for X-ray absorption spectroscopy using IFEFFIT, J. Synchrotron Radiat. 12 (2005) 537–541. doi:10.1107/S0909049505012719.
[30] R Core Team, R: A language and environment for statistical computing, (2015). http://www.R-project.org/.
[31] J. Oksanen, F.G. Blanchet, R. Kindt, P. Legendre, P.R. Minchin, R.B. O'Hara, et al., vegan: Community Ecology Package. R package version 2.2-1., (2015). http://CRAN.R-project.org/package=vegan.
[32] W.N. Venables, B.D. Riplay, Modern Applied Statistics with R, Fourth, Springer, New York, 2002.
[33] E. Seeger, A. Baun, M. Kastner, S. Trapp, Insignificant acute toxicity of TiO2 nanoparticles to willow trees, J. Soils Sediments. 9 (2009) 46–53. doi:10.1007/s11368-008-0034-0.
[34] D.L. Jacob, J.D. Borchardt, L. Navaratnam, M.L. Otte, A.N. Bezbaruah, Uptake and translocation of Ti from nanoparticles in crops and wetland plants, Int J Phytoremediation. 15 (2013) 142–53. doi:10.1080/15226514.2012.683209.
[35] A.S. Foltete, J.F. Masfaraud, E. Bigorgne, J. Nahmani, P. Chaurand, C. Botta, et al., Environmental impact of sunscreen nanomaterials: ecotoxicity and genotoxicity of altered TiO2 nanocomposites on Vicia faba, Env. Pollut. 159 (2011) 2515–22. doi:10.1016/j.envpol.2011.06.020.

548 [36] C. Larue, J. Laurette, N. Herlin-Boime, H. Khodja, B. Fayard, A.M. Flank, et al., Accumulation,
549 translocation and impact of TiO2 nanoparticles in wheat (Triticum aestivum spp.): influence of
550 diameter and crystal phase, Sci Total Env. 431 (2012) 197–208.
551 doi:10.1016/j.scitotenv.2012.04.073.
552 [37] C. Larue, G. Veronesi, A.M. Flank, S. Surble, N. Herlin-Boime, M. Carriere, Comparative uptake
553 and impact of TiO(2) nanoparticles in wheat and rapeseed, J Toxicol Env. Health A. 75 (2012)
554 722–734. doi:10.1080/15287394.2012.689800.
555 [38] P. Thuesombat, S. Hannongbua, S. Akasit, S. Chadchawan, Effect of silver nanoparticles on rice
556 (Oryza sativa L. cv. KDML 105) seed germination and seedling growth, Ecotoxicol. Environ. Saf.
557 104 (2014) 302–309. doi:10.1016/j.ecoenv.2014.03.022.
558 [39] L.Y. Yin, Y.W. Cheng, B. Espinasse, B.P. Colman, M. Auffan, M. Wiesner, et al., More than the
559 Ions: The Effects of Silver Nanoparticles on Lolium multiflorum, Environ. Sci. Technol. 45 (2011)
560 2360–2367. doi:10.1021/es103995x.
561 [40] U. Song, H. Jun, B. Waldman, J. Roh, Y. Kim, J. Yi, et al., Functional analyses of nanoparticle
562 toxicity: a comparative study of the effects of TiO2 and Ag on tomatoes (Lycopersicon
563 esculentum), Ecotoxicol. Environ. Saf. 93 (2013) 60–67. doi:10.1016/j.ecoenv.2013.03.033.
564 [41] D.A. Notter, D.M. Mitrano, B. Nowack, Are nanosized or dissolved metals more toxic in the
565 environment? A meta-analysis, Environ. Toxicol. Chem. SETAC. 33 (2014) 2733–2739.
566 doi:10.1002/etc.2732.
567 [42] E. Navarro, F. Piccapietra, B. Wagner, F. Marconi, R. Kaegi, N. Odzak, et al., Toxicity of silver
568 nanoparticles to Chlamydomonas reinhardtii, Environ. Sci. Technol. 42 (2008) 8959–8964.
569 doi:10.1021/es801785m.
570 [43] A.G. González, S. Mombo, J. Leflaive, A. Lamy, O.S. Pokrovsky, J.-L. Rols, Silver nanoparticles
571 impact phototrophic biofilm communities to a considerably higher degree than ionic silver,
572 Environ. Sci. Pollut. Res. Int. 22 (2015) 8412–8424. doi:10.1007/s11356-014-3978-1.
573 [44] C. Beer, R. Foldbjerg, Y. Hayashi, D.S. Sutherland, H. Autrup, Toxicity of silver nanoparticles -
574 nanoparticle or silver ion?, Toxicol. Lett. 208 (2012) 286–292. doi:10.1016/j.toxlet.2011.11.002.
575 [45] N. Lubick, Nanosilver toxicity: ions, nanoparticles--or both?, Environ. Sci. Technol. 42 (2008)
576 8617–8617. doi:10.1021/es8026314.
577 [46] D. McShan, P.C. Ray, H. Yu, Molecular toxicity mechanism of nanosilver, J. Food Drug Anal. 22
578 (2014) 116–127. doi:10.1016/j.jfda.2014.01.010.
579 [47] M. Khodakovskaya, E. Dervishi, M. Mahmood, Y. Xu, Z.R. Li, F. Watanabe, et al., Carbon
580 nanotubes are able to penetrate plant seed coat and dramatically affect seed germination and
581 plant growth, Acs Nano. 3 (2009) 3221–3227. doi:10.1021/nn900887m.
582 [48] S. Leclerc, K.J. Wilkinson, Bioaccumulation of Nanosilver by Chlamydomonas reinhardtii-
583 nanoparticle or the free ion?, Environ. Sci. Technol. 48 (2014) 358–364. doi:10.1021/es404037z.
584 [49] D.E. Salt, I. Baxter, B. Lahner, Ionomics and the Study of the Plant Ionome, Annu. Rev. Plant
585 Biol. 59 (2008) 709–733. doi:10.1146/annurev.arplant.59.032607.092942.
586 [50] H. Qian, X. Peng, X. Han, J. Ren, L. Sun, Z. Fu, Comparison of the toxicity of silver nanoparticles
587 and silver ions on the growth of terrestrial plant model Arabidopsis thaliana, J. Environ. Sci.
588 China. 25 (2013) 1947–1955. doi:10.1016/S1001-0742(12)60301-5.
589 [51] K. Varmuza, P. Filzmoser, Introduction to Multivariate Statistical Analysis in Chemometrics, CRC
590 Press, 2009.
591 [52] R. Rousseau, Detection limit and estimate of uncertainty of analytical XRF results, Rigaku J. 18
592 (2001) 33–47.
593 [53] A.D. Servin, H. Castillo-Michel, J.A. Hernandez-Viezcas, B.C. Diaz, J.R. Peralta-Videa, J.L. Gardea-
594 Torresdey, Synchrotron Micro-XRF and Micro-XANES Confirmation of the Uptake and
595 Translocation of TiO2 Nanoparticles in Cucumber (Cucumis sativus) Plants, Environ. Sci.
596 Technol. 46 (2012) 7637–7643. doi:10.1021/es300955b.
597 [54] A.D. Servin, M.I. Morales, H. Castillo-Michel, J.A. Hernandez-Viezcas, B. Munoz, L. Zhao, et al.,
598 Synchrotron verification of TiO2 accumulation in cucumber fruit: a possible pathway of TiO2

599 nanoparticle transfer from soil into the food chain, Env. Sci Technol. 47 (2013) 11592–11598.
600 doi:10.1021/es403368j.
601 [55] C.O. Dimkpa, J.E. McLean, N. Martineau, D.W. Britt, R. Haverkamp, A.J. Anderson, Silver
602 nanoparticles disrupt wheat (Triticum aestivum L.) growth in a sand matrix, Env. Sci Technol. 47
603 (2013) 1082–1090. doi:10.1021/es302973y.
604 [56] R.G. Haverkamp, A.T. Marshall, The mechanism of metal nanoparticle formation in plants: limits
605 on accumulation, J. Nanoparticle Res. 11 (2009) 1453–1463. doi:10.1007/s11051-008-9533-6.
606 [57] J.L. Gardea-Torresdey, E. Gomez, J.R. Peralta-Videa, J.G. Parsons, H. Troiani, M. Jose-Yacaman,
607 Alfalfa Sprouts: A Natural Source for the Synthesis of Silver Nanoparticles, Langmuir. 19 (2003)
608 1357–1361. doi:10.1021/la020835i.
609